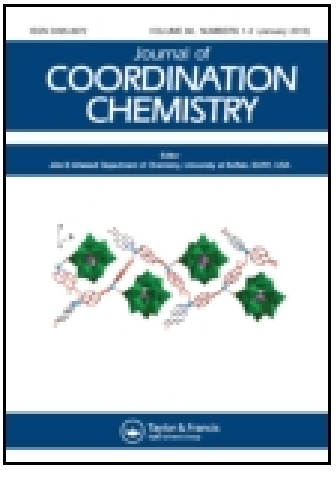

Journal of Coordination Chemistry
Publication details, including instructions for authors and subscription information:
http://www.tandfonline.com/loi/gcoo20

Rhenium(II) nitrosyl complexes: synthesis, characterization, DFT calculations and DNA nuclease activity

Swapna Ghosh[ab], Shiv Shankar Paul[a], Joyee Mitra[c] & Kalyan K. Mukherjea[a]

[a] Department of Chemistry, Jadavpur University, Kolkata, India

[b] Department of Chemistry, Sreegopal Banerjee College, Hooghly, India

[c] Department of Chemistry, IIT Kanpur, Kanpur, India

Accepted author version posted online: 28 May 2014.Published online: 18 Jun 2014.

To cite this article: Swapna Ghosh, Shiv Shankar Paul, Joyee Mitra & Kalyan K. Mukherjea (2014) Rhenium(II) nitrosyl complexes: synthesis, characterization, DFT calculations and DNA nuclease activity, Journal of Coordination Chemistry, 67:10, 1809-1834, DOI: 10.1080/00958972.2014.924622

To link to this article: http://dx.doi.org/10.1080/00958972.2014.924622

Journal of Coordination Chemistry, 2014
Vol. 67, No. 10, 1809–1834, http://dx.doi.org/10.1080/00958972.2014.924622

Rhenium(II) nitrosyl complexes: synthesis, characterization, DFT calculations and DNA nuclease activity

SWAPNA GHOSH†‡, SHIV SHANKAR PAUL†, JOYEE MITRA§ and KALYAN K. MUKHERJEA*†

†Department of Chemistry, Jadavpur University, Kolkata, India
‡Department of Chemistry, Sreegopal Banerjee College, Hooghly, India
§Department of Chemistry, IIT Kanpur, Kanpur, India

(*Received 5 October 2013; accepted 1 April 2014*)

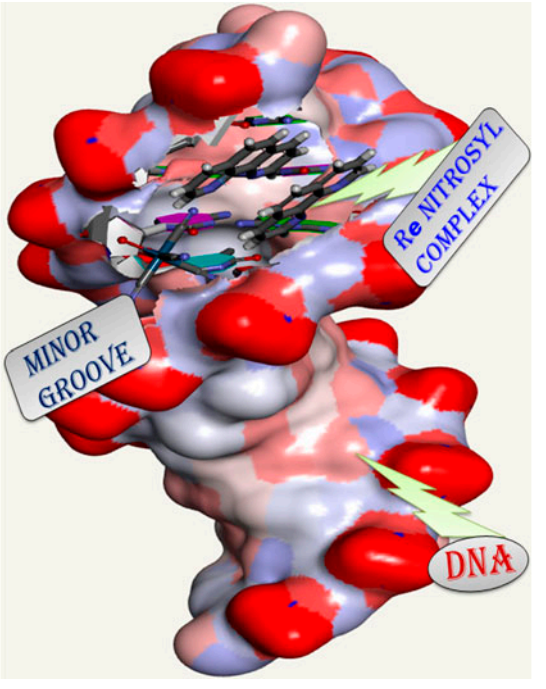

The synthesis of mono and dinitrosyl rhenium(II) complexes were done. Mono nitrosyl complex was characterized by single crystal X-ray diffraction, which was further supported by DFT and Hirshfeld surface analysis. DNA binding and nuclease activity of both complexes were performed.

*Corresponding author. Email: kkmukherjee@chemistry.jdvu.ac.in
S. Ghosh and S.S. Paul have contributed equally to this work.

The rhenium(II) dinitrosyl and mononitrosyl complexes, i.e. $[Re(NO)_2(CN)_4]\cdot(Phen)_2\cdot 2H_2O$ (**1**) and $PhenH[Re(NO)(CN)_4(H_2O)]\cdot(Phen)\cdot 3H_2O$ (**2**) have been isolated and characterized. The X-ray crystal structure of **2** reveals that Re(II) is octahedrally coordinated with one nitrosyl, four cyanides, and one water, with one phenanthroline protonated to compensate the charge of the Re(II) center. The crystal structure shows chemically significant non-covalent interactions like hydrogen bonding involving the uncoordinated water and π–π interactions between phenanthrolinium and phen. The structures of both complexes have been optimized by DFT. Absorption and emission spectral studies and viscosity measurements indicate that both **1** and **2** interact with calf thymus DNA through partial intercalation of DNA bases. The intrinsic-binding constants, obtained from UV–vis spectroscopic studies, are 1.2×10^4 and $7.2 \times 10^4\ M^{-1}$ for **1** and **2**, respectively. Both **1** and **2** are capable of inducing cleavage of plasmid DNA in the presence of H_2O_2 to form the supercoiled form to nicked circular form. The spectroscopic results of DNA binding are supported by molecular docking studies.

Keywords: Rhenium(II) nitrosyl complexes; DFT study; Hirshfeld surface analysis; DNA binding study; Molecular docking

1. Introduction

Syntheses of metal complexes which can bind nucleic acids received attention for diverse applications in various fields of chemistry [1, 2]. DNA is generally the primary intracellular target of anticancer drugs, which are usually small molecules (small planar heteroaromatic cations are useful and important intercalators). The interaction between small molecules and DNA can help to understand the death of cell or apoptosis [3, 4]. Nitrogen containing planar hetero-aromatic cations like ethidium bromide (EB), a polycondensate benzophenanthridine (3, 8-di-amide substituted), has been well known as a DNA intercalator and used as a probe to identify new intercalators. Binding of transition metal complexes having planar aromatic ligands with DNA has generated interest, owing to their possible applicability as new cancer therapeutic agents. Inorganic compounds that are capable of inducing cleavage in DNA have been termed as inorganic nucleases. Developing inorganic nucleases that can be exploited as potential substitutes for natural nuclease enzymes for monitoring DNA structure and conformations is necessary. Hence, it has become imperative to develop synthetic, sequence-selective DNA binding, and cleavage agents for DNA itself and for new potential DNA targeting antitumor drugs [5–7].

Nitric oxide plays a key role in human cardiovascular and nervous systems and a vital role in defense mechanisms against micro-organisms and tumor cells [8–11]. It has been suggested that the one-electron redox relatives of NO, the nitrosonium cation (NO^+), the nitroxide anion (NO^-), and the conjugate acid of NO^-, nitroxyl (HNO), are responsible for some aspects of the biological chemistry of nitric oxide [12–17]. Metal nitrosyl complexes have drawn considerable interest due to their fascinating coordination chemistry [18, 19], and their potential application as antitumor and antiseptic agents, in catalysis, and in photochemical processes [20–24]. Due to the prominence of the oxo group, coordination chemistry of Re(V) in terms of structures, geometries, reactivity, redox processes, and magnetic properties has become stagnant, resulting in restriction of a variety of rhenium-based therapeutic agents for cancer treatment [25]. Thus, further development of new potential rhenium-based therapeutic agents will largely depend on the discovery of new stable rhenium-coordinated moieties.

Synthesis and characterization of rhenium nitrosyl complexes and their interaction with DNA have been accomplished and are being reported herein. From a DFT study, IR

stretching frequencies were also calculated using gas phase-optimized geometries in the ground state. The nuclease activities of two rhenium nitrosyl complexes in the presence of H_2O_2 were monitored using pUC19 DNA. The DNA-binding mode was confirmed further by a docking study for **2**, as the crystal structure of **2** was solved.

2. Materials and experimental methods

2.1. *Materials*

The starting material, $K[ReO_4]$, was of extra pure quality and obtained from Aldrich. Hydroxylamine hydrochloride was of extra pure quality and obtained from Sisco Research Laboratory (India). Potassium cyanide was obtained from s.d. Fine Chem. Ltd (India). Potassium hydroxide pellets and methanol (G.R.) were products of Merck (India) and were used directly. All other chemicals were obtained from Merck (India). The analytical grade solvents used for physico-chemical studies were further purified by literature methods before use, wherever necessary. CT-DNA was purchased from Sigma Chemical Company, USA; supercoiled (SC) plasmid pUC19 DNA was obtained from Bangalore Genei, India.

2.2. *Physical measurements for characterization of the complexes*

UV–vis spectra were recorded on a Shimadzu U-1700 spectrophotometer and IR spectra (KBr disk) were recorded on a Perkin-Elmer IR spectrophotometer. Electrical conductivity in a DMF solution was measured with a Systronics 304 digital conductivity meter at 10^{-3} M dm^{-3}. Magnetic susceptibilities were obtained from a vibrating sample magnetometer PAR 155 model. Microanalytical (C, H, N) data were collected on a Perkin-Elmer 2400C elemental analyzer. ESR spectra were measured in DMF solution at 77 K using a Varian EPR-4 spectrophotometer. All pH measurements were made with an Elico (India) digital pH meter.

2.3. *Synthesis of rhenium(II) nitrosyl complexes*

2.3.1. Preparation of solution A. $KReO_4$ (0.1 g, 0.35 mM), KCN (0.23 g, 3.5 mM), and KOH (0.6 g, 10.5 mM) were dissolved in a minimum volume of hot water (ca. 90 °C) and solid NH_2OH (0.36 g, 5.25 mM) was added to the solution, portion wise with continuous stirring. After 5 min, a crimson solution was obtained. Stirring was continued while heating for another 1h to drive out the evolved NH_3 from the solution. The solution was then cooled and its pH was adjusted to ca. 3 by slow addition of dilute HCl, keeping the temperature of the solution below 10 °C (solution A).

2.3.2. Preparation of $[Re(NO)_2(CN)_4]\cdot(Phen)_2\cdot 2H_2O$ (1). The cold acidified solution A was added dropwise, with stirring, to a hot aqueous solution of 1,10-phenanthroline (0.21 g, 1.16 mM; dissolved in 10 mL of hot water). The stirring was continued for 25 min, when the color of the solution turned light orange to yellow and on cooling to room temperature a brown compound precipitated which was filtered off, washed thoroughly with water and acetone and dried in vacuum. The brown compound was soluble only in DMF and DMSO from which diffraction grade crystals could not be obtained despite innumerable attempts.

Yield: 0.10 g (20%). Anal. Calcd for $C_{28}H_{20}N_{10}O_4Re$: C, 46.2; H, 2.27; N, 16.6. Found: C, 45.9; H, 2.8; N, 16.32. IR (KBr disk, cm^{-1}): 2090(vs), 2130(sh), 2016(m) [υ(CN)]; 1730(s), 1700(vs) [υ(NO)]; 620(m) [υ(Re–N(NO)]; 350, 405(w) [υ(Re–N(ligand)]; 460(m) [υ(Re–C)], UV–vis: λ_{max}/nm ($\varepsilon'/M^{-1}\,cm^{-1}$): 741(705), 444(495); 323(2432); 264(9142); ESI-MS (*m/z*): 718 [$C_{28}H_{16}N_{10}O_2Re$].

2.3.3. Preparation of PhenH[Re(NO)(CN)$_4$(H$_2$O)]·(Phen)·3H$_2$O (2). After separation of the dinitrosyl compound, the orange–yellow filtrate was collected into a beaker and to that filtrate anhydrous Na_2SO_4 was added portion wise until an orange yellow mass separated. The product was filtered off and the orange yellow filtrate was collected in a beaker and was set aside for 48 h, when dark red shiny diffraction grade crystals separated, were filtered off, washed with water and ethanol and dried in a vacuum. The compound was highly soluble in DMSO and slightly soluble in DMF. Yield: 0.05 g (10%). Anal. Calcd for $C_{28}H_{25}N_9O_5Re$: C, 46.9; H, 2.7; N, 16.2. Found: C, 46.6; H, 2.8; N, 16.3. IR (KBr disk, cm^{-1}): 2080(vs), 2120(sh) [υ(CN)]; 1736(vs) [υ(NO)]; 620(m) [υ(Re–N(NO)]; 350,405(w) [υ(Re–N(ligand)]; 460(m) [υ(Re–C)], UV–vis: λ_{max}/nm ($\varepsilon'/M^{-1}\,cm^{-1}$): 424(129); 354 (1155); 265(7428).

2.4. *X-ray crystallographic details*

The crystal structure of the Re-complex **2** was obtained by single-crystal X-ray diffraction. All geometric and intensity data were collected at room temperature using an automated Bruker SMART APEX CCD diffractometer equipped with a fine focus 1.75 kW sealed tube Mo -Kα X-ray source ($\lambda = 0.71073$ Å). All data were corrected for Lorentz and polarization effects [26]. Empirical absorption correction was also applied. The structure was solved by combination of Patterson and Fourier techniques and refined by full-matrix least-squares using the SHELX system of programs [27]. All hydrogens belonging to the complex other than for water were placed in their calculated positions and refined with a riding model. All non-hydrogen atoms were refined anisotropically. Perspective views of the molecules were obtained by ORTEP [28].

2.5. *Hirshfeld surface analysis*

Hirshfeld surfaces are becoming valuable tools for analyzing intermolecular interactions in the crystal structures, and are constructed on the basis of electron distribution calculated as the sum of spherical atom electron densities [29, 30]. The Hirshfeld surface is unique for a given crystal structure [31] as it is the property of the intermolecular interactions of molecular crystals. The Hirshfeld surface enclosing a molecule is defined by points where the contribution to the electron density from the molecule of interest is equal to the contribution from all other molecules. The Hirshfeld surfaces represented by d_{norm}, shape index, curvedness, and 2-D fingerprint plots were generated using Crystal Explorer 2.1 [32]. Graphical plots of the molecular Hirshfeld surfaces were made with d_{norm} using a red, white, and blue color scheme, where red represents shorter contacts, white is used for contacts around the van der Waals separation, and blue is for longer contacts. Two further colored properties (shape index and curvedness) established on the local curvature of the surface can be specified [33]. The distances in the iso-surface are defined as d_e and d_i, where d_e is the distance

from the point to the nearest nucleus external to the surface and d_i is the distance from the point to the nearest nucleus internal to the surface. The normalized contact distance (d_{norm}) based on both d_e and d_i, and the van der Waals radii (vdW) of the atom, are given by equation:

$$d_{norm} = (d_i - r_i^{vdW})/r_i^{vdW} + (d_e - r_e^{vdW})/r_e^{vdW} \quad (1)$$

The value of d_{norm} is negative or positive when intermolecular contacts are shorter or longer than van der Waals separations. Because of the symmetry between d_e and d_i in the expression for d_{norm}, where two Hirshfeld surfaces touch, both will display a red spot identical in color intensity as well as size and shape. The combination of d_e and d_i in the form of a 2-D fingerprint plot provides summary of intermolecular contacts in the crystal [34].

2.6. *DFT calculation*

DFT calculations were performed using Gaussian 03 (Revision D.01) [35] package. The method used was Becke's three-parameter hybrid-exchange functional, and the nonlocal correlation provided by Lee, Yang, and Parr expression, as well as the Vosko, Wilk and Nuair's 1980 local correlation functional (III) (B3LYP) [36]. Unrestricted calculation (UB3LYP) was performed in both cases. 6-31G*+ basis set [37] was used for carbon, nitrogen, oxygen, and hydrogen atoms. The LANL2DZ basis set and LANL2 pseudopotentials of Hay and Wadt were used for Re [38]. Single point calculations were done in DMSO using the Klamt's form of the conductor reaction field (COSMO) [39] solvent models. Assignment of each MO was done on the basis of its composition as calculated from the AOMix program [40] and by visual inspection of its localized orbital. Optimized minima were characterized by harmonic-vibration-frequency calculation with the same method and basis set in which the minimum has no imaginary frequency. Initial geometry of the Re-mono nitrosyl complex was taken from the crystal structure and used without further optimization. The structure of Re-dinitrosyl was optimized starting from a guessed structure. Single point calculations and population analysis of molecular orbitals were carried out by taking *xyz* coordinates of optimized geometries. Molecular orbitals were visualized using "Gauss View". The assignment of the type of each MO was made on the basis of its composition and by visual inspection of its localized orbital.

2.7. *DNA-binding study*

The present project is directed towards development of synthetic nitrosyl-based nucleases. DNA damage can be imparted primarily through DNA binding and damage in the presence of H_2O_2. So, to establish the efficacy of complexes as DNA nuclease, the DNA binding and their subsequent role in DNA nuclease in the presence of H_2O_2 were studied. A control experiment with phen and the analogous di-anionic Re nitrosyl complex $[Re(NO)(CN)_5]^{2-}$ [41(a)] were performed to compare the activity of the present compounds.

2.7.1. Electronic absorbance spectral study. Stock solution of CT-DNA was prepared by dissolving DNA in Tris–HCl/NaCl buffer solution and stored at 4 °C. The resultant homogeneous solution was used within four days. The concentration of CT-DNA per nucleotide

phosphate was calculated by following a literature method [42]. The purity of DNA was checked by monitoring the absorbance ratio at 260 and 280 nm [43]. UV–vis spectra were recorded in a Shimadzu U-1700 spectrophotometer. A control-binding experiment was performed using phen with CT-DNA to understand the effect of free phen. Again, a comparative-binding experiment was performed using the di-anionic Re nitrosyl complex with CT-DNA. During absorption titration experiments, a fixed concentration of **1** or **2**, phen and the di-anionic Re-complex $[Re(NO)(CN)_5]^{2-}$ (20 µL) was titrated with increasing amounts of DNA from 20 to 200 µL with appropriate blank for each titration. The intrinsic equilibrium DNA-binding constants (K_b) of the complexes to CT-DNA were determined by monitoring the change of the absorption intensity of the spectral bands with increasing concentration of CT-DNA using equation [44]:

$$[DNA]/(\varepsilon_a - \varepsilon_f) = [DNA]/(\varepsilon_b - \varepsilon_f) + 1/[K_b(\varepsilon_b - \varepsilon_f)] \quad (2)$$

Here, [DNA] is the concentration of DNA in base pairs, the apparent absorption coefficients ε_a, ε_f, and ε_b correspond to A_{obsd}/[complex], the extinction coefficient for the free complex, and the extinction coefficient for the complex in the fully bound form, respectively. Plots of $[DNA]/(\varepsilon_a - \varepsilon_f)$ *versus* [DNA] gave a slope of $1/(\varepsilon_b - \varepsilon_f)$ with a *Y*-intercept of $1/[K_b\ (\varepsilon_b - \varepsilon_f)]$. The intrinsic-binding constant K_b was obtained from the ratio of the slope to the intercept.

2.7.2. Fluorescence emission titrations. Emission intensity measurements were carried out using a Perkin Elmer LS-55 spectrofluorimeter. Relative binding of the Re–NO complexes to CT-DNA were studied by fluorescence spectral technique using the binding of EB to CT-DNA solution in Tris–HCl/NaCl buffer (pH 7.2) [45]. A control and comparative experiments were also performed using phen and $[Re(NO)(CN)_5]^{2-}$ with CT-DNA. In this binding experiment, 60 µM of CT-DNA solution in Tris–HCl/NaCl buffer (50 mM Tris–HCl and 50 mM NaCl, pH 7.2) was added to 90 µM of EB in the same buffer medium to get the maximum fluorescence intensity. Aliquots of 1.0 mM stock solution of **1**, **2**, or di-anionic Re-complex $[Re(NO)(CN)_5]^{2-}$ in DMF and phen in methanol were added in the range 0–140 µM to the EB bound CT-DNA solution and the fluorescence was measured after each addition. The solutions were excited at 500 nm (with excitation and emission slit 10 nm) and spectra were recorded from 510 to 700 nm.

2.7.3. Viscometric studies. Viscometric titrations were done using a fabricated microviscometer maintained at 28 (±0.5) °C in a thermostated water bath. The CT-DNA was sonicated [46] (average molecular weight of ~200 base pairs using a Labsonic 2000 sonicator) and the flow times were measured with a stopwatch. Each sample was measured three times and an average flow time was calculated. The relative solution viscosity (η/η_0) was estimated from the relation $(L/L_0) = (\eta/\eta_0)^{1/3}$, where (L/L_0) is the contour length and L_0 and η_0 denote the apparent molecular length and solution viscosity, respectively, in the absence of the metal complex. The viscosity data were presented as $(\eta/\eta_0)^{1/3}$ *versus* [complex]/[DNA], where η is the viscosity of DNA in the presence of the complex and η_0 that of DNA alone. Viscosity values were obtained from the observed flow time of DNA containing solutions (t) corrected for that of the buffer alone (t_0), $\eta = t - t_0$.

2.7.4. Gel electrophoresis study. The DNA cleavage activity of the complexes was monitored using agarose gel electrophoresis wherein the SC pUC19 DNA (0.2 μg per reaction) in Tris–HCl buffer (50 mM) with 50 mM of NaCl (pH 7.2) was treated with 20 μM H_2O_2 and solutions of different concentrations of metal complex followed by dilution with the Tris–HCl buffer to a total volume of 15 μL which were then incubated for 1 h at 37 °C. After incubation it was mixed with loading buffer containing 25% bromophenol blue, 30% glycerol (3 μL), and was finally loaded on 0.9% agarose gel containing 1.0 μg mL^{-1} EB. Electrophoresis was carried out at 80 V for 3 h in TAE buffer (Tris, acetic acid, EDTA, pH 7.2). Bands were visualized by UV light and photographed. The extent of SC pUC19 DNA cleavage induced by the complex was determined by measuring the intensities of the bands using UVP Bio Doc IT Gel Imaging System.

2.7.5. Molecular docking. The rigid molecular docking studies were performed using HEX 6.3 software [47] (http://www.loria.fr/~ritchied/hex/). This is an interactive molecular graphics program for calculating and displaying feasible docking modes of a drug with proteins, enzymes, and DNA. The coordinates of the metal complex were taken from its crystal structure as a CIF file and converted to the PDB format using Mercury software (http://www.ccdc.cam.ac.uk/). The crystal structure of the B-DNA dodecamer d $(CGCGAATTCGCG)_2$ (PDB ID: 1BNA) was downloaded from the protein data bank (http://www.rcsb.org./pdb). All calculations were carried out on an Intel I5, 3.1 GHz-based machine running MS Windows 7 as operating system. Visualization of the docked pose has been done using Discovery studio 3.1 and PyMol (http://pymol.sourceforget.net/) molecular graphics program.

3. Results and discussion

3.1. *Synthetic aspect of the complexes*

ReO_4^- and $NH_2OH{\cdot}HCl$ react in the presence of CN^- in alkaline medium giving a densely colored solution, which when treated with phen after bringing the pH of the solution down to three, generated a mixture of rhenium nitrosyl moieties. Firstly $[Re(NO)_2(CN)_4]{\cdot}(Phen)_2{\cdot}2H_2O$ (**1**) containing the $[Re(NO)_2]^{2+}$ moiety was separated, thereafter the filtrate afforded an orange–yellow mass by addition of Na_2SO_4, possessing $PhenH[Re(NO)(CN)_4(H_2O)]{\cdot}(Phen){\cdot}3H_2O$ (**2**) with the $[Re(NO)]^{3+}$ moiety. Molecular weights for **1** and **2** were determined in DMF using vapor pressure osmometric method. The ESI-MS (*m/z*) for **1** was found to be 718 (M^+) $[C_{28}H_{16}N_{10}O_2Re]$. Complexes **1** and **2** are monomeric in DMF. The molar conductance data of the complexes show that **2** is a 1 : 1 electrolyte and **1** is a non-electrolyte as expected from their molecular formulas.

3.2. *Spectroscopic characterization of the complexes*

The dinitrosyl complex **1** shows two υNO vibrations at 1730 and 1700 cm^{-1}, whereas the mononitrosyl complex **2** shows υNO at 1736 cm^{-1}. For metal dinitrosyl complexes having a *trans* geometry of two nitrosyl (NO) groups, only one υNO is obtained in IR spectra, while with *cis* geometry of the NO ligands, both the symmetric and anti-symmetric

stretching vibrations are IR active [48]. The symmetric vibration occurs at higher energy than the anti-symmetric stretching vibration. Complexes **1** and **2** in the solid state possess sharp but split υCN bands at 2090, 2016, and 2080, 2020 cm^{-1}, respectively [48]. Another band at 620 cm^{-1} in both **1** and **2** is due to the υReN (NO) vibration. Other bands due to phen in these complexes are not significantly modified from those of free phen. The water molecules present in **1** and **2** are characterized by intense υOH at ca. 3400 cm^{-1}. The δH_2O vibration in both complexes is, however, embedded within the intense υNO absorption. Assuming NO^+ formalism [19(b), 48], the formal oxidation state of rhenium should be +2 ($5d^5$) in both **1** and **2**. Thus, both complexes are paramagnetic (corresponding to one unpaired electron), which confirms that the metal nitrosyl moieties for **1** and **2** can be represented as $\{Re(NO)_2\}^V$ and $\{Re(NO)\}^V$, respectively. The slightly high μ_{eff} value for **1** and **2** (ca. 2.2 BM) compared to the spin-only value may be due to the high negative (low spin d^5) value of the spin-orbit coupling constant of rhenium.

Complex **1** shows low energy intense electronic transitions centered at 741 nm in DMF, which are absent in **2**. The broad spectrum from 300 to 400 nm for both complexes is common. Both **1** and **2** are six coordinate and may possess comparable molecular symmetry in so far as the two nitrosyl groups in **1** are *cis* [49]. So, this difference in absorption spectrum may be due to the fact that **1** possess $\{Re(NO_2)\}^V$, while **2** possess $\{Re(NO)\}^V$ moieties.

Both rhenium complexes are EPR active (figures 1 and 2). The spectra are highly anisotropic with respect to both $<g>$ and $<A>$ tensors. While rhenium hyperfine (both 185 and 187; Re has $I = 5/2$) are prominent, but the spacing pattern clearly shows the lowering of the size of both the types of $<A>$ tensors in going from parallel to the perpendicular direction [50]. There appears a ^{14}N super hyperfine triplet (A ca. 40G) in both cases in the vicinity of $g_\perp$. The details of the EPR parameters derived from figures 1 and 2 are shown in table 1.

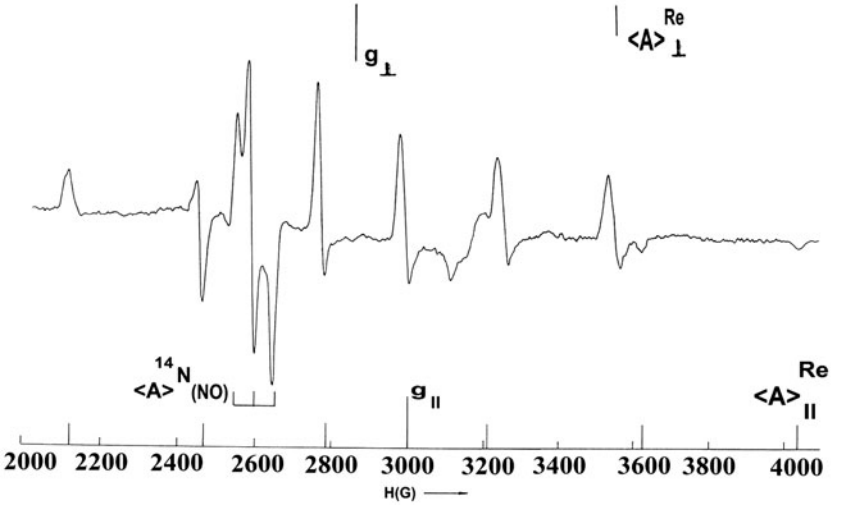

Figure 1. EPR spectrum of **1** at 77 K.

Table 1. EPR parameters of **1** and **2**.

Compound	$\langle g\rangle_{\perp}$	$\langle g\rangle_{\parallel}$	$\langle g\rangle_{av}$	Re$\langle A\rangle_{\perp}$/ *G*	Re$\langle A\rangle_{\perp}$/ *G*	Re$\langle A\rangle_{iso}$	N$\langle A\rangle$ $\langle NO\rangle$/*G*
1. $[Re(NO)_2(CN)_4](Phen)_2\cdot 3H_2O$	2.34	1.98	2.22	70–320	460–560	200–400	40
2. (PhenH)[Re(NO) $(CN)_4\cdot H_2O]\cdot(Phen)\cdot 3H_2O$	2.28	2.19	2.25	125–315	320–425	190–352	40

3.3. *Crystal structure*

The molecular structure of **2** has been determined by single-crystal X-ray diffraction analysis (table 2) and selected bond lengths and angles are listed in tables 3–5. The ORTEP view of the complex is shown in figure 3. Complex **2** crystallizes in the monoclinic $P2_1/c$ space group, and the asymmetric unit consists of one $[Re(NO)(CN)_4(H_2O)]^-$, phenanthroline cation, one neutral phen, and three solvent waters. The rhenium center is connected to a nitrogen of nitrosyl, four carbons of CN^-, and one water with a distorted octahedral geometry. The average Re–N (NO) bond distance of 1.779 Å is similar to the one reported in other mononitrosyl complexes [51–53]. The Re–C [2.0461(11)–2.1588(7) Å] and C–N [1.3003 (15)–1.714(12) Å] bond lengths are comparable to the corresponding values reported for related complexes. The Re–OH_2 bond distance of 2.243(1) Å in **2** agrees well with the 2.165(5) Å observed in $(AsPh_4)_2[Re(NO)(H_2O)(CN)_4]\cdot 5H_2O$ [41]. The average Re–N–O bond angle of 172.2(14) is close to linear, indicating that the nitrosyl moieties exhibit sp hybridized NO^+ character in **2** [54]. The phen molecules in **2** with expected N–C and C–C bond lengths are nearly planar. The crystal packing diagram of **2** reveals a layering effect in which different layers interact by π–π stacking and H-bonding interactions (figure 4). Phenanthroline cation (A) moiety is stacked with the planar phen (B) present in the crystal lattice through π–π interactions. The distance between A and B is 3.526 Å and with the

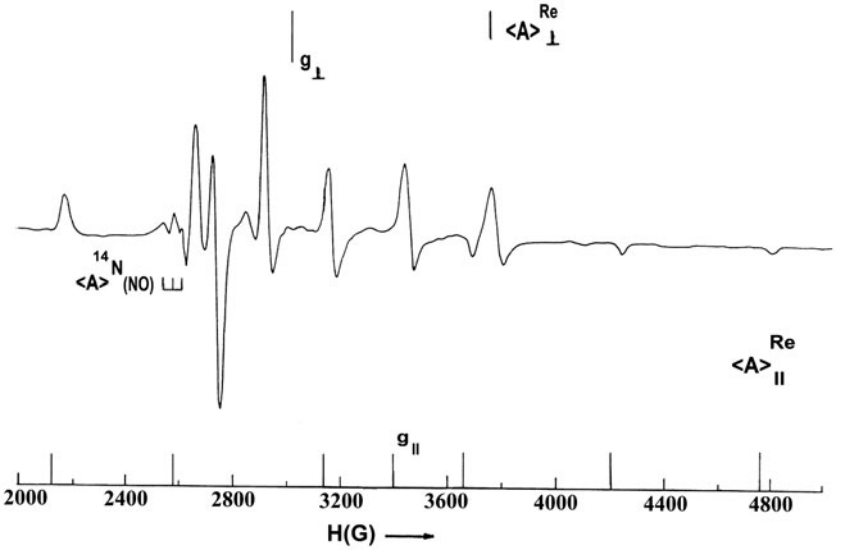

Figure 2. EPR spectrum of **2** at 77 K.

Table 2. Crystal data and structure refinement parameters of **2**.

Parameters	
Empirical formula	C12 H8 N2, C12 H9 N2, C4 N5 O2 Re, 3(O)
M_r	745.72
T/K	293(2)
λ/Å	0.71073
Crystal system	Monoclinic
Space group	*P21/c*
Unit cell dimensions	
a/Å	7.1392(6)
b/Å	13.9079(11)
c/Å	30.587(2)
α/°	90.00
β/°	102.873(2)
γ/°	90.00
V/Å^3, Z	2960.7(4)
D_{Calcd}/g cm^{-3}	2, 1.673
F (0 0 0)	1452
Crystal size/mm	0.05 × 0.08 × 0.14
θ Range for data collection (°)	2.0, 27.7
Reflections collected	48,050
Independent reflections (R_{int})	6872(0.051)
Completeness to $\theta = \theta_{max}$ (%)	99.4
Refinement method	Full-matrix least-squares on F^2
Data/restraints/parameters	6872/0/388
Goodness-of-fit on F	1.081
Final R indices [$I > 2\sigma(I)$]	$R_1 = 0.0737$, $wR_2 = 0.1200$
R indices (all data)	$R_1 = 0.0782$, $wR_2 = 0.1204$
Largest diff. peak, hole/Å^{-3}	−4.26, 2.45

C moiety is 3.719 Å (figure 4), indicating that there exists strong π–π stacking interactions between the two phenanthroline moieties. The supramolecular crystal packing structure is formed based on these associated interactions which stabilize the crystal lattice.

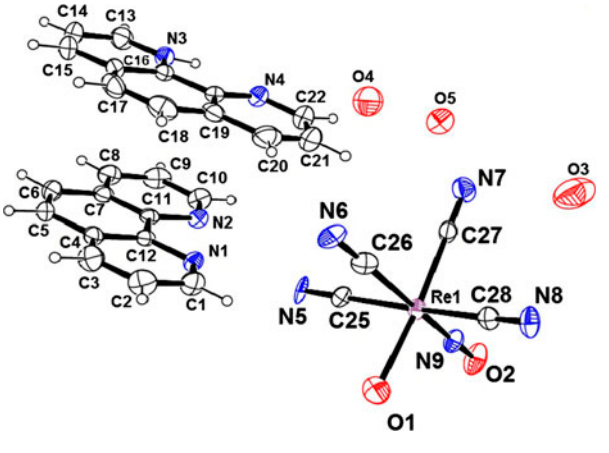

Figure 3. The ORTEP view of **2** with ellipsoids of 45% probability.

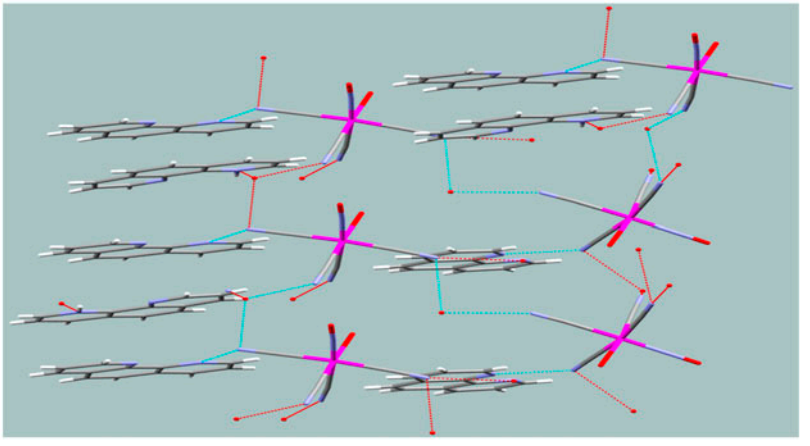

Figure 4. Packing pattern showing the H-bonding and π–π stacking interactions of **2**.

3.4. *Hirshfeld surface analysis*

The Hirshfeld surfaces of **2** are presented in figure 5 showing surfaces that have been mapped over d_{norm} [figure 5(A)] range −0.5 to 1.5 Å, shape index [figure 5(B)] range from −1.0 to 1.0 Å, and curvedness [figure 5(C)] from −4.0 to 0.4 Å. The surfaces are shown as transparent to allow visualization of the molecular moiety, in a similar orientation for all structures, around which they were calculated. The dominant interactions between N···H and O···H in **2** can be seen in the Hirshfeld surface as the red areas in figure 6. Other visible spots in the Hirshfeld surfaces correspond to H···H contacts. The small extent of area and light color on the surface indicate weaker and longer contacts other than hydrogen bonds. The O···H/H···O and N···H/H···N intermolecular interactions appear as distinct spikes in the 2-D fingerprint plot (figure 6) in **2**. Complementary regions are visible in the fingerprint plots, where one molecule is a donor ($d_e > d_i$) and the other an acceptor ($d_e < d_i$).

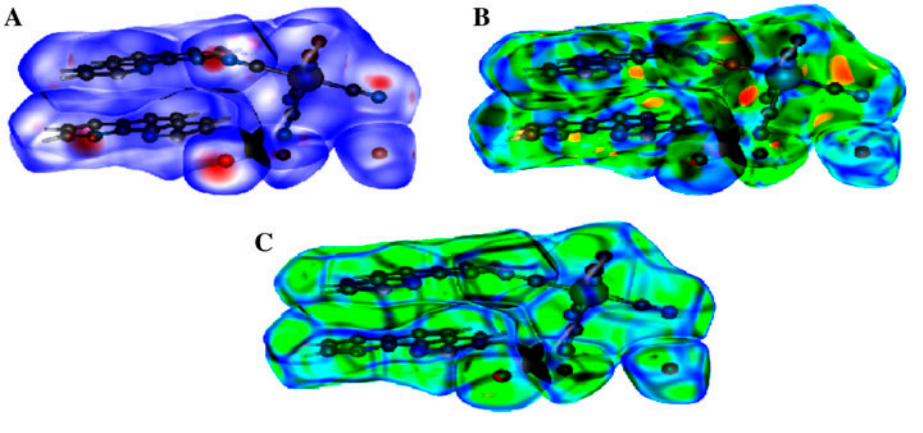

Figure 5. Hirshfeld surface mapped with (A) d_{norm}, (B) shape index, (C) curvedness for **2**.

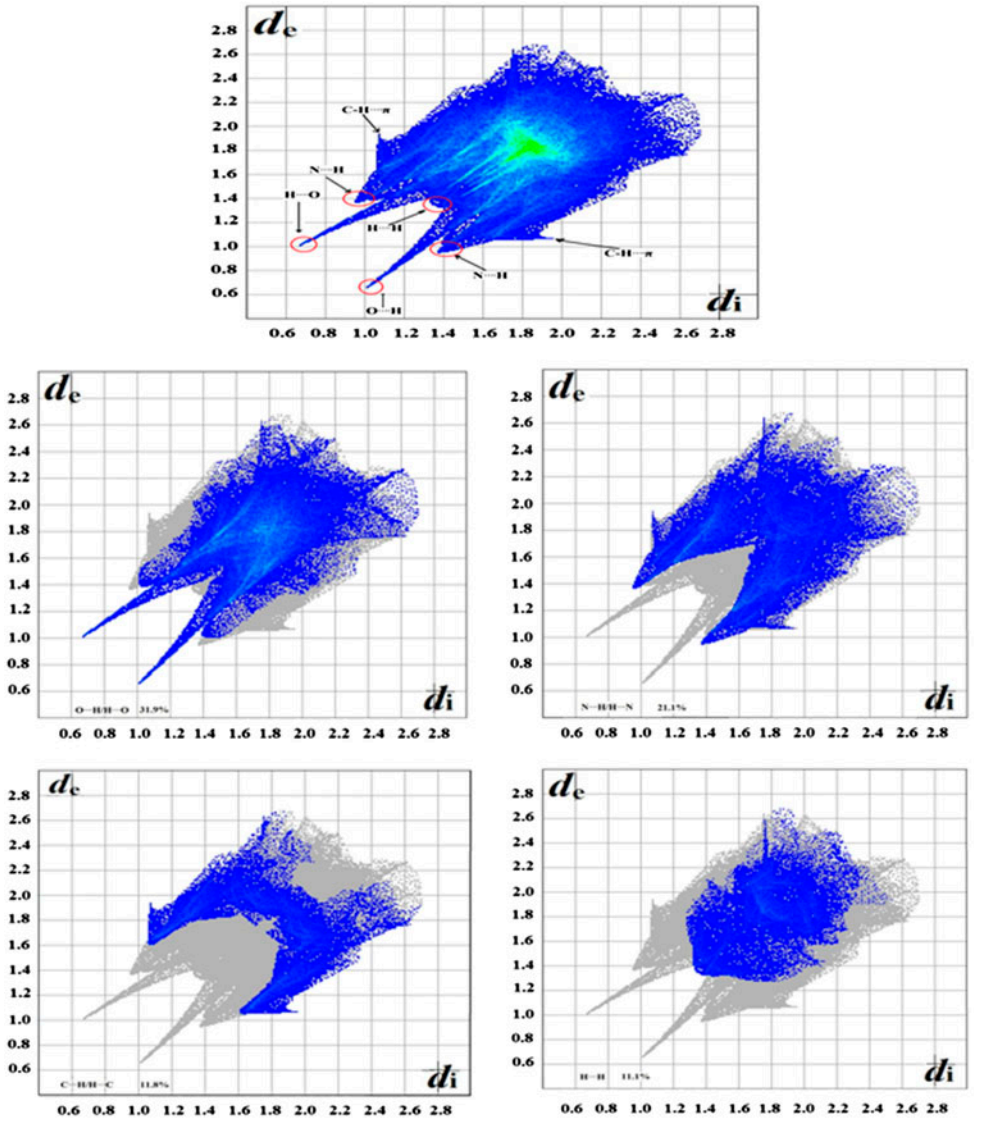

Figure 6. Fingerprint plot of **2**: full and resolved into N···H, O···H, C···H and H···H contacts showing the percentages of contacts contributed to the total Hirshfeld surface area of molecules.

The fingerprint plots can be decomposed to highlight particular atom pair close contacts [29]. This decomposition enables separation of contributions from different interaction types, which overlap in the full fingerprint plot. In the 2-D fingerprint plots, two distinct spikes appear for O···H/H···O intermolecular interactions. The proportion of O···H/H···O interactions comprises 31.9% of the total Hirshfeld surfaces for each molecule of **2**. The upper spike corresponding to the donor represents the O···H interactions ($d_i = 0.664$, $d_e = 1.010$ Å in **2**) and the lower spike being an acceptor represents the H···O interactions

($d_e = 0.664$, $d_i = 1.010$ Å in **2**) in the fingerprint plot (figure 6 for **2**). For N···H/H···N intermolecular interactions, two distinct spikes appear in the 2-D fingerprint plot, and the proportion of interactions involve 21.1% of the total Hirshfeld surfaces for each molecule of **2**. The upper spike corresponding to the donor represents the N···H interactions ($d_i = 0.946$, $d_e = 1.362$ Å in **2**) and the lower spike being an acceptor represents the H···N interactions ($d_e = 0.946$, $d_i = 1.362$ Å in **2**) in the fingerprint plot. There are characteristic "wings" in the plot which are identified as a result of C–H···π interactions [29–31, 55]. The decomposition of the fingerprint plot shows that C···H/H···C contacts comprise 11.8% of the total Hirshfeld surface area for **2**. The region corresponds to all C–H···C interactions of which C–H···π appears in the fingerprint plot in a characteristic manner. From the Hirshfeld surface, the adjacent red and blue triangles on the shape index surface shows that the π–π stacking interaction is almost identical to that of the crystal structure. The pattern of red and blue triangles in the same region of the shape index surface is another characteristic of π···π interactions. Blue triangles represent convex regions due to ring carbons of the molecule inside the surface, while red triangles represent concave regions due to carbons of the π-stacked molecule above it. The contribution of H···H interactions to the Hirshfeld surface for **2** is 11.1%. The relative contribution of the different interactions to the Hirshfeld surface was calculated for **2**, and these interactions can be attributed to different supramolecular synthons, leading to diverse crystal packing arrangements.

3.5. *Density functional theoretical calculations*

The single point calculations for both complexes have been carried out in the presence of DMSO as the dielectric medium. The dinitrosylated complex is more stable in solution (i.e. of lower energy). Thus, the structure of this complex has been optimized from DFT calculations (figures 7(A) and 7(B)). In the mononitrosylated complex, one N of phenanthroline is

Table 3. Selected bond lengths (Å) of **2**.

Re(1)–C(27)	2.046(8)	N(6)–C(26)	1.108(10)
Re(1)–C(28)	2.090(7)	N(7)–C(27)	1.148(10)
Re(1)–C(25)	2.090(7)	N(8)–C(28)	1.171(9)
Re(1)–C(26)	2.159(9)	N(3)–H(3A)	0.9850
Re(1)–O(1)	2.224(7)		
Re(1)–N(9)	1.779(6)		
N(9)–O(2)	1.187(7)		
N(5)–C(25)	1.150(9)		

Table 4. Selected bond angles (°) of **2**.

O(1)–Re(1)–N(9)	96.4(3)	C(25)–Re(1)–C(26)	87.3(3)
O(1)–Re(1)–C(25)	87.8(3)	C(25)–Re(1)–C(27)	90.9(3)
O(1)–Re(1)–C(26)	85.9(3)	C(25)–Re(1)–C(28)	169.3(3)
O(1)–Re(1)–C(27)	172.3(3)	C(26)–Re(1)–C(27)	86.5(3)
O(1)–Re(1)–O(28)	88.7(3)	C(26)–Re(1)–C(28)	82.4(3)
N(9)–Re(1)–C(25)	97.7(3)	C(27)–Re(1)–C(28)	91.3(3)
N(9)–Re(1)–C(26)	174.6(3)	C(24)–N(3)–H(3A)	121.5
N(9)–Re(1)–C(27)	91.33(3)	C(13)–N(3)–H(3A)	116.5
N(9)–Re(1)–C(28)	92.8(3)	Re(1)–N(9)–O(2)	176.5(6)

Table 5. Relevant hydrogen bonds in **2**.

D–H···A	d(D–H)	d(H···A)	d(D···A)	∠(DHA)
N(3)–H(3A)···O(5)	0.99	1.71	2.6349(5)	155
C(5)–H(5)···O(2)	0.93	2.56	3.4097(6)	151
C(9)–H(9)···N(5)	0.93	2.48	3.3684(7)	159
C(14)–H(14)···N(7)	0.93	2.61	3.4213(8)	147

protonated. From the frontier orbital analysis, for mononitrosylated complex, the α-SOMO (HOMO) is based on nitrogen of phenanthroline which is not protonated. The protonated phenanthroline is not involved in the SOMO formation. Its corresponding β orbital is principally based on the rhenium *d*-orbital and remains unpopulated due to its higher energy (−4.50 eV for β compared to −6.34 eV for α). The electron density distribution in the

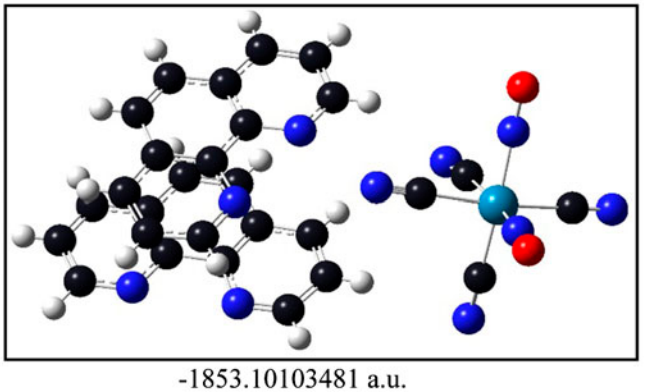

Figure 7(A). DFT optimized structure of $[Re(NO)_2(CN)_4]$ (**1**).

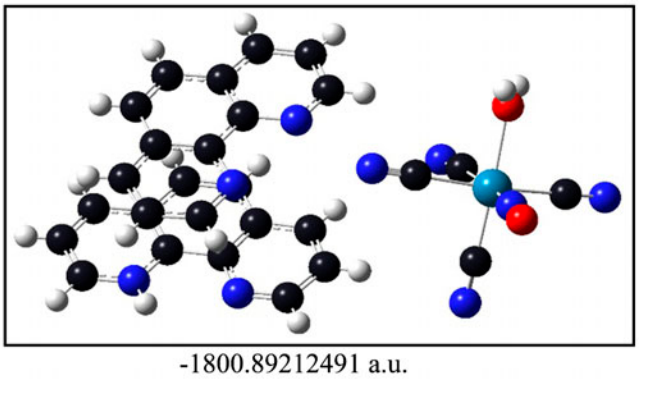

Figure 7(B). DFT optimized structure of $PhenH[Re(NO)(CN)_4(H_2O)]$ (**2**).

LUMO (both α and β) is delocalized over the protonated phenanthroline. Here, α and β orbitals are energetically almost degenerate [figure 8(A)].

In case of the dinitrosylated complex, the difference in electron density distribution is different from the previous case. The α-SOMO (HOMO) is based on nitrogen of phenanthroline. Its unoccupied β counterpart shows electron density distribution delocalized over phenanthroline and considerable contribution from one nitrogen from the second phenanthroline. The α-HOMO (−7.05 eV) is considerably stabilized compared to its β counterpart (−6.03 eV) as observed in the previous complex. The LUMO (both α and β) is located almost entirely on the two coordinated nitrosyl ligands. Here, also the α and β orbitals (LUMO) are energetically almost degenerate. No participation of rhenium d orbital is

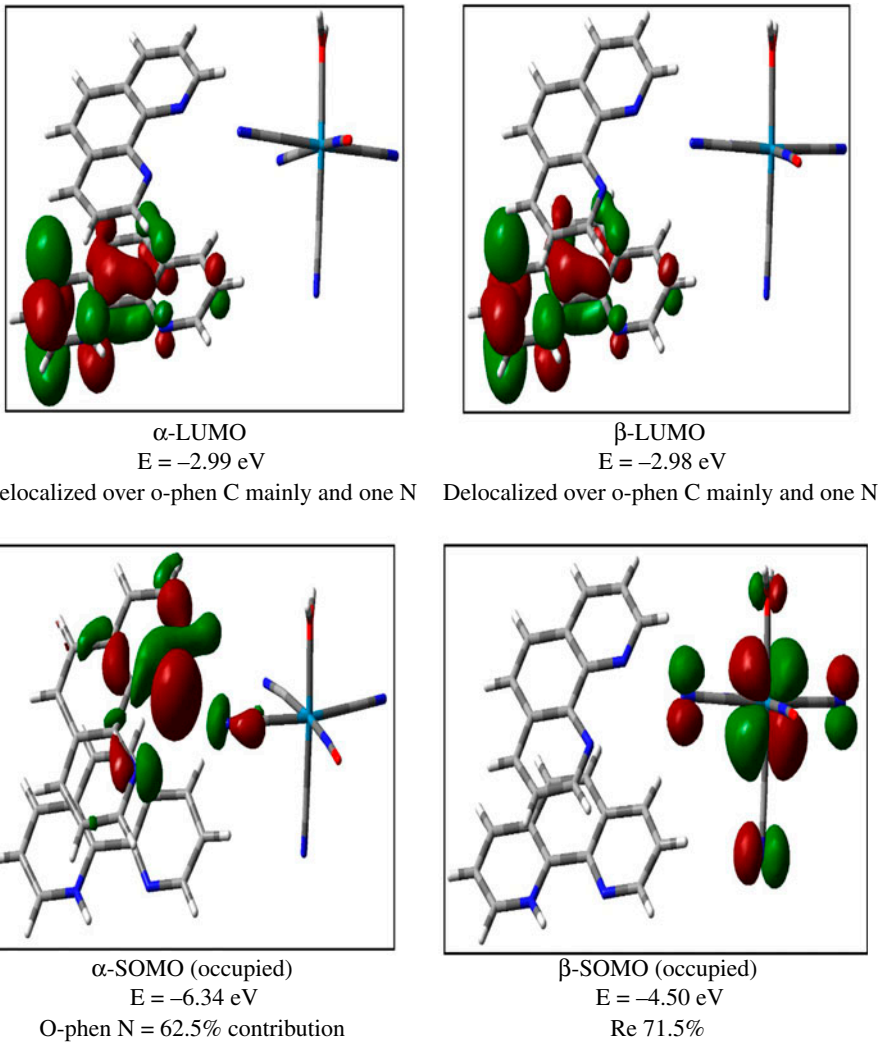

Figure 8(A). Contour plots and energy of the α-spin LUMO and β-spin LUMO orbitals and α-SOMO (occupied) and β-SOMO (unoccupied) orbitals of **2**.

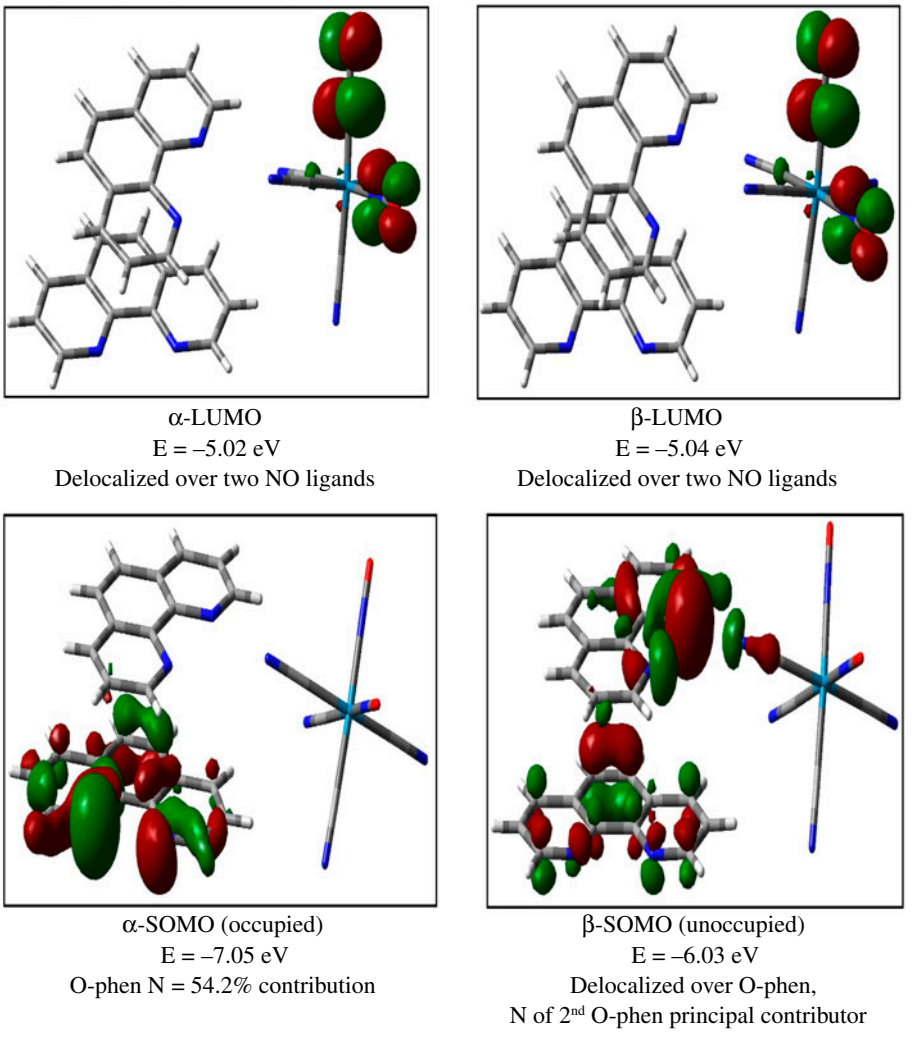

Figure 8(B). Contour plots and energy of the α-spin LUMO and β-spin LUMO orbitals and α-SOMO (occupied) and β-SOMO (unoccupied) orbitals of **1**.

observed in the frontier orbitals of this complex [figure 8(B)]. The structure of the dinitrosyl complex was further supported by IR frequency calculations, which were obtained by DFT. The two υNO vibrations at 1738 and 1816 cm^{-1} and for υCN frequency at 2145 and 2329 cm^{-1} (figure 9) obtained from the DFT calculations are within the tolerance limit with the value obtained experimentally (table 6).

3.6. *DNA-Re complex interaction study*

3.6.1. Electronic absorption spectroscopy. The determination of overall binding constants by monitoring the changes in absorption of the metal complexes induced by the

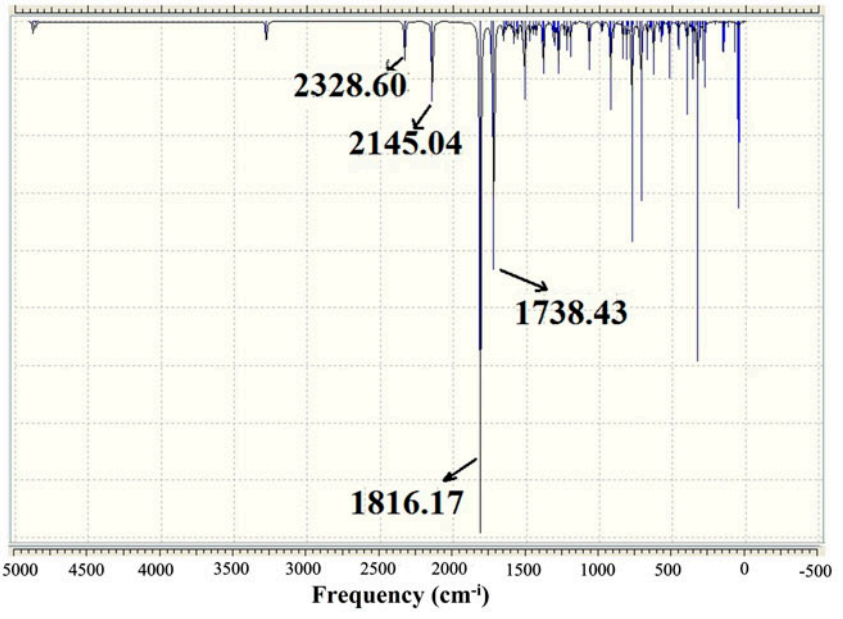

Figure 9. IR spectrum of **1** from DFT study.

addition of increasing amounts of CT-DNA is one of the most widely used techniques [56–58]. Addition of calf thymus DNA to **1** and **2** induced a decrease, i.e. hypochromism in absorption bands (235–340 nm), indicating strong binding of these complexes with DNA. The hypochromicity suggests that the complex might bind to the minor groove of DNA by a partial intercalation, due to a strong interaction between electronic states of the intercalating chromophore and those of the DNA bases. The intrinsic-binding constants of the complexes with CT-DNA were obtained using equation (2) by monitoring the changes in absorption at 264 and 265 nm for **1** and **2**, respectively (figures 10 and 11), as 1.2×10^4 and $7.2 \times 10^4\ M^{-1}$ for **1** and **2**, respectively. The control experiment was performed monitoring the 264 nm band of phen and 268 nm band of the di-anionic Re-nitrosyl complex $[Re(NO)(CN)_5]^{2-}$ by titrating against CT-DNA (figures 12 and 13). The intrinsic-binding constants of the phen and di-anionic Re nitrosyl complex with CT-DNA were 0.2×10^3 and 1.4×10^4 M^{-1}. It is clear that the binding affinity of **1** and **2** was greater than phen alone and comparable to the di-anionic analog. The value of the binding constant K_b for **1** and **2** suggests that the mode of binding to CT-DNA is partial intercalation [59].

Table 6. Comparisons of experimental and theoretical stretching frequency of **1**.

Frequency	Theoretical values (cm^{-1})	Experimental values (cm^{-1})	% of deviation
υ NO(i)	1700	1738.43	2.3
υ NO(ii)	1730	1816.04	4.98
υ CN(i)	2016	2145.04	6.4
υ CN(ii)	2090	2328.60	11.4

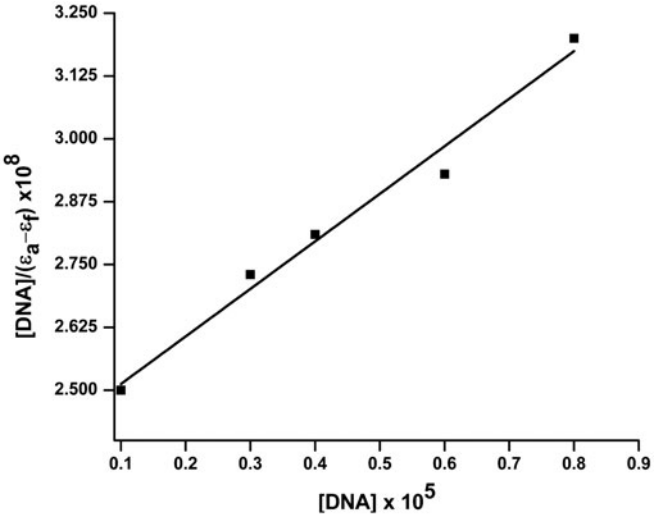

Figure 10. Plot of $[DNA]/(\varepsilon_a - \varepsilon_f) \times 10^8$ M/M^{-1} cm^{-1} *vs.* [DNA] $\times 10^5$ M for **1**.

3.6.2. EB displacement assay. The fluorimetric competitive binding experiment was carried out using EB as a probe, which has feeble emission intensity in water. However, the emission intensity of EB is greatly enhanced in the presence of DNA due to its strong intercalation between adjacent DNA base pairs [60]. The competitive intercalative binding of another small molecule to CT-DNA could result in displacement of EB, characterized by quenching of the fluorescence of EB [61]. When phen, **1**, **2**, and $[Re(NO)(CN)_5]^{2-}$ were added to DNA pretreated with EB, the DNA-induced emission intensity of EB at 587 nm of the DNA-EB system gradually decreased (figures 14 and 15) with increasing concentration

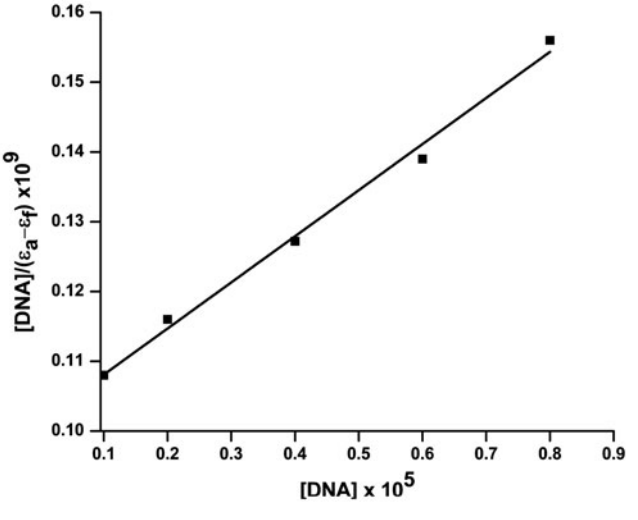

Figure 11. Plot of $[DNA]/(\varepsilon_a - \varepsilon_f) \times 10^9$ M/M^{-1} cm^{-1} *vs.* [DNA] $\times 10^5$ M for **2**.

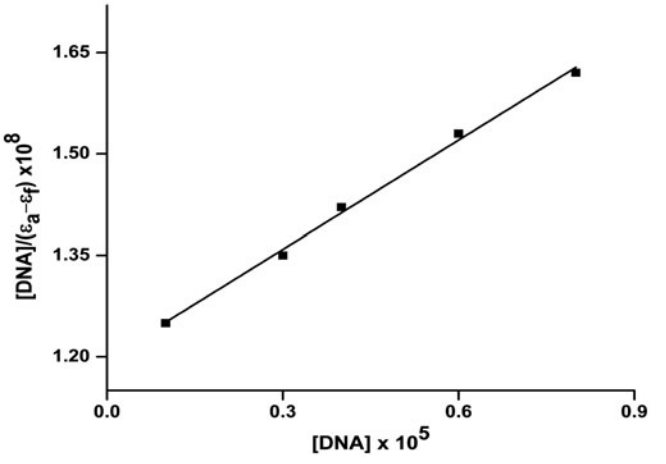

Figure 12. Plot of $[DNA]/(\varepsilon_a - \varepsilon_f) \times 10^9$ M/M^{-1} cm^{-1} *vs.* $[DNA] \times 10^5$ M for phen.

of phen and complexes. The changes observed here are characteristic of intercalation. So, phen, di-anionic Re-nitrosyl complex, **1**, and **2** compete with EB in the binding of DNA.

The metal complex-induced fluorescence quenching was analyzed further by the Stern–Volmer equation [62]:

$$I_0/I = I + K_{sv}[Q] \tag{3}$$

where I_0 and I represent the fluorescence intensities in the absence and presence of the complexes, respectively, and $[Q]$ is the concentration of the complexes. K_{sv} is a linear Stern–Volmer quenching constant which is obtained experimentally from the slope of I_0/I

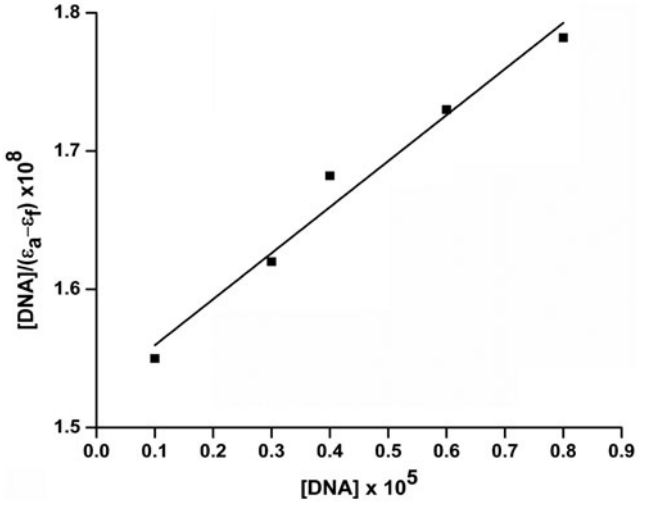

Figure 13. Plot of $[DNA]/(\varepsilon_a - \varepsilon_f) \times 10^9$ M/M^{-1} cm^{-1} *vs.* $[DNA] \times 10^5$ M for dianionic Re-complex.

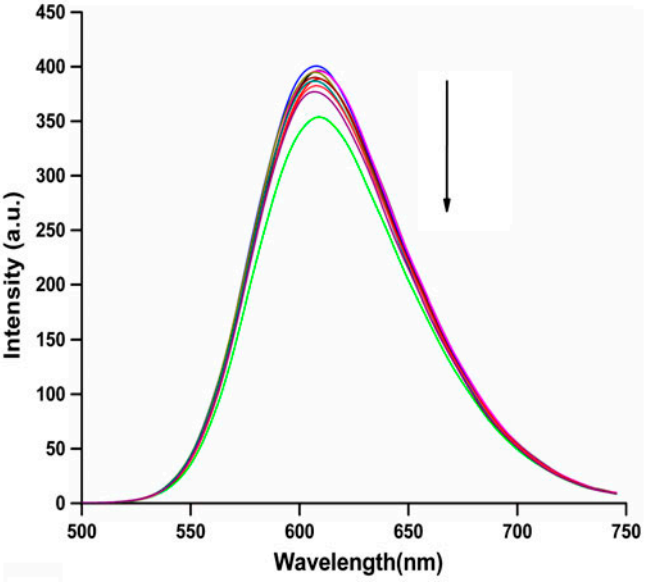

Figure 14. Effect of addition of **1** (0–140 μM) to the emission intensity of the DNA bound EB.

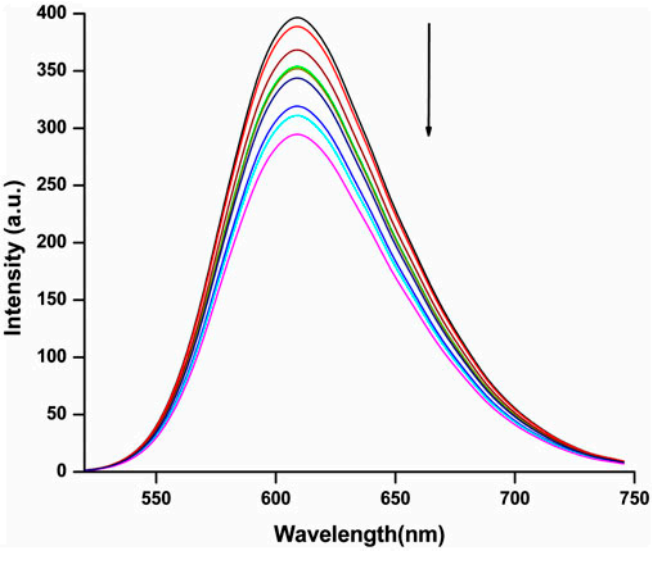

Figure 15. Effect of addition of **2** (0–140 μM) to the emission intensity of the DNA bound EB.

versus [*Q*]. From the plot (figure 16), the K_{sv} values for phen, di-anionic Re-nitrosyl complex, **1**, and **2** are 1.5×10^3, 4.7×10^4, 3.5×10^4, and $1.5 \times 10^5\ M^{-1}$, respectively, which suggests that the interaction of the complexes with DNA is moderately strong [63].

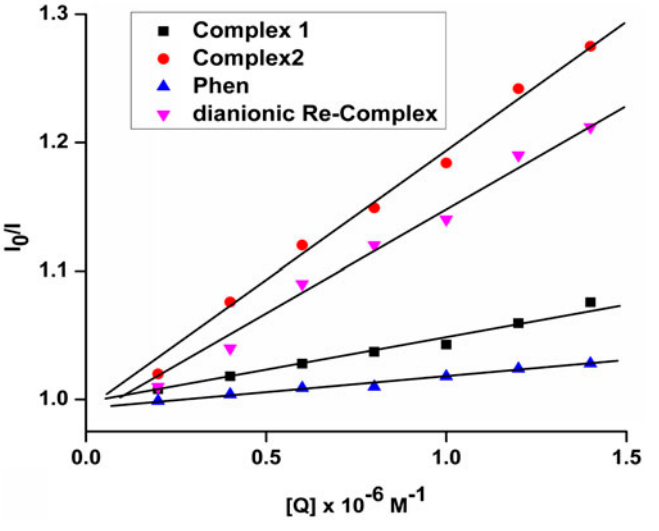

Figure 16. Stern–Volmer plot for **1**, **2**, phen and dianionic Re-complex.

3.6.3. Viscometric studies for assessing the DNA-binding pattern. Hydrodynamic measurements, mainly viscosity, are sensitive techniques to determine DNA-binding modes. The relative viscosity of CT-DNA solution increases by the intercalative binding of substrates. The intercalation of any small molecule between the DNA base pairs causes a lengthening of the DNA helix, resulting in an increase in the intrinsic viscosity; partial or non-classical binding of ligand may bend or kink the DNA helix, thereby decreasing its effective length and subsequently viscosity [64, 65]. The values of relative specific viscosities of DNA in the absence and presence of phen, $[Re(NO)(CN)_5]^{2-}$, **1**, and **2** are plotted against [complex]/[DNA] (figure 17). Addition of phen and complexes to CT-DNA solution leads to an increase in the viscosity of the CT-DNA, which clearly demonstrates intercalative binding.

3.6.4. Nuclease activity. The nuclease activity of **1** and **2** in the presence of H_2O_2 has been studied using SC pUC19 DNA in DMF–Tris buffer containing NaCl (pH 7.2). The nuclease activity of some metal complexes in the presence of hydrogen peroxide is attributed to participation of hydroxyl radicals in DNA cleavage [66]. The naturally occurring SC form (form I), when nicked, gives an open circular-relaxed form (form II), whereas relatively fast migration is observed for form I, while form II migrates slowly. Figure 18 shows the electrophoretic pattern of plasmid DNA treated with **1** and **2**. The present experiment suggests that untreated DNA and DNA incubated with peroxide alone did not show any significant DNA cleavage (Lanes 1–2). However, in the presence of peroxide, **1** and **2** were found to exhibit good nuclease activity (table 7). In the presence of H_2O_2 as an oxidizing agent, oxidation of the metal complex takes place that leads to formation of more accessible and reactive oxygen species ($OH^{\bullet}$) by the Fenton-type mechanism [67], causing DNA cleavage. It is observed that **2** (mono-nitrosyl complex) is more effective in nicking pUC19 DNA either alone or in combination with H_2O_2 than the dinitrosylated complex. This can

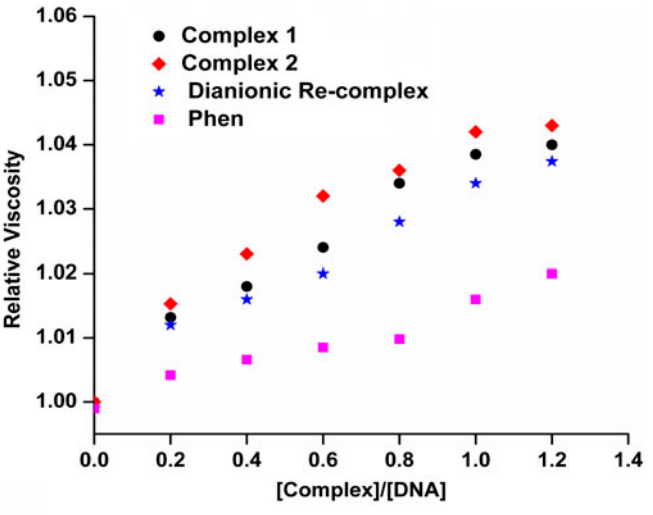

Figure 17. Effect of increasing amount of **1**, **2**, phen and dianionic Re-complex on the relative viscosity of CT-DNA. Samples were prepared to give total complex/base pair ratios of 0.2, 0.4, 0.6, 0.8, 1.0 and 1.2.

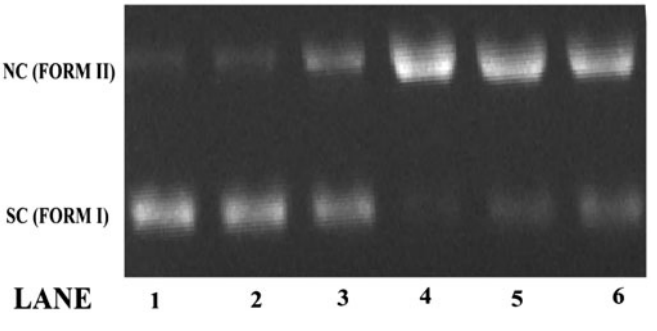

Figure 18. Agarose gel (0.9%) electrophoregram of SC pUC19 DNA (0.2 μg) incubated for 45 min at 37 °C in a buffer containing 50 mM Tris–HCl and 50 mM NaCl at 37 °C pH 7.2, 20 μM H_2O_2 and with increasing complex concentrations.

Table 7. Extent of DNA SC pUC19 cleavage by the complexes.

Lane no.	Reaction condition	Form I (% SC)	Form II (% NC)
1	DNA CONTROL	90	10
2	DNA + 20 μM H_2O_2	85	15
3	DNA + 20 μM H_2O_2 + 10 mM Complex **1**	75	25
4	DNA + 20 μM H_2O_2 + 50 mM Complex **1**	35	65
5	DNA + 20 μM H_2O_2 + 10 mM Complex **2**	60	40
6	DNA + 20 μM H_2O_2 + 50 mM Complex **2**	48	52

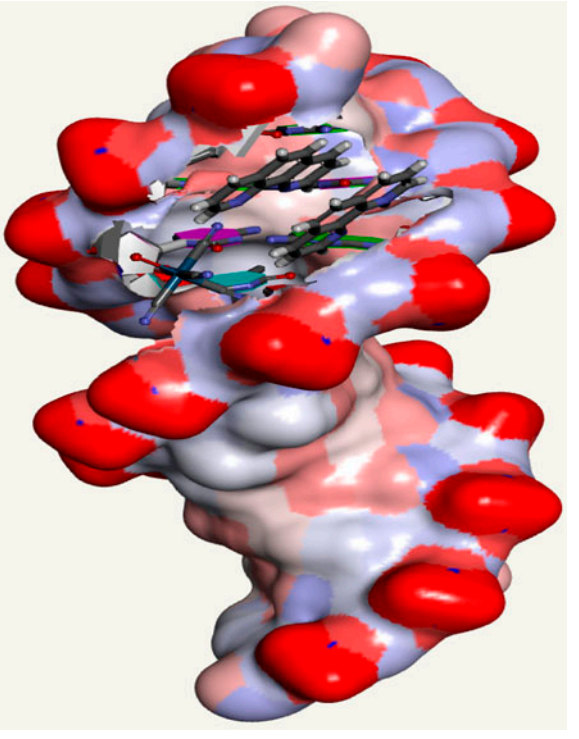

Figure 19. Docked pose of **2** with DNA.

be attributed to the fact that as the stability of the dinitrosyl complex in solution is high (vide DFT calculation), it reacts slowly in the solution phase to induce nicking of DNA.

3.6.5. Molecular docking of complex 2 with DNA. To understand the DNA-drug interactions, a molecular docking study provides information regarding the interaction, i.e. the nature of binding, binding affinity, and binding site of DNA. The mechanistic study places a small molecule into the binding site of the target-specific region of DNA mainly in a non-covalent fashion, although a covalent bond may also be formed with the reactive ligand, to predict the correct binding mode and binding affinities [68]. Different structural properties lead to different binding modes; in fact, one of the most important factors governing the binding mode is the molecular shape. The forces maintaining the stability of the DNA-intercalator complex include van der Waals, hydrogen bonding, hydrophobic, charge transfer, and electrostatic complementarity [69, 70]. In our experiment, **2** was successively docked with DNA duplex of sequence d(CGCGAATTCGCG)$_2$ dodecamer (PDB ID: 1BNA) to predict the chosen binding site along with preferred orientation of the ligand inside the DNA minor groove. The lowest binding energy conformer was searched out of six different conformers for each docking simulation and the resultant one was used for further analysis. The energetically most favorable conformation of the docked pose (figure 19) revealed that **2** strongly binds to the minor groove of DNA [71] and slightly bends the DNA in such a way that a part of the planar phenanthroline ring makes favorable

stacking interactions between DNA base pairs, which lead to van der Waals interaction with the DNA functional groups that define the stability of the groove. An electrostatic interaction also exists between the cationic core of phenanthroline ion and anionic oxygen of the phosphate backbone of DNA double helix. The resulting relative binding energy of docked structure was $-293.8\,\mathrm{kJ\,mol^{-1}}$, which indicates the more potent binding affinity between DNA and **2**, correlating well with the experimental DNA-binding studies. Thus, the results obtained from the docking study are well harmonized with results obtained from spectroscopic experiments.

4. Conclusion

Two nitrosyl complexes of rhenium, i.e. di-nitrosyl and mono-nitrosyl complexes, are synthesized and characterized. The mononitrosyl complex, **2**, is structurally characterized by single X-ray crystallography. The structures of both the complexes were optimized by DFT calculations. The DFT study shows the optimized structure of dinitrosyl complex is in excellent agreement with the proposed structure. The Hirshfeld surface is used to visualize the reliability of the computed crystal structure. The nature of the intermolecular interactions present in **2** is more easily understood using Hirshfeld surface analysis. In the present study, the interaction of **1** and **2** with CT-DNA is examined by absorbance and fluorescence spectroscopy, as well as viscometric methods. The results of control and comparative experiment suggest that binding of **1** and **2** with CT-DNA is of partial intercalation. The absorbance studies reveal that the intrinsic-binding constants for **1** and **2** are 1.2×10^4 and $7.2 \times 10^4\,\mathrm{M^{-1}}$, respectively. Furthermore, in the EB competition fluorescence assay, the Stern–Volmer quenching constant for these complexes, K_{sv}, were 3.5×10^4 and 1.5×10^5 $\mathrm{M^{-1}}$, respectively, which suggests that the complexes bind moderately to DNA as intercalator by competitive displacement of EB. The complexes exhibit effective nuclease activity in the presence of H_2O_2 by cleaving the SC plasmid (pUC19) DNA to nicked circular one. The molecular docking study supports binding of **2** to DNA where the relative binding energy of the lowest docked structure is $-293.8\,\mathrm{kJ\,M^{-1}}$.

Supplementary material

CCDC 878568 contains the supplementary crystallographic data for **2**. These data can be obtained free of charge via http://www.ccdc.cam.ac.uk/deposit or from the Cambridge Crystallographic Data Center, 12 Union Road, Cambridge CB2 1EZ, UK; Fax: (+44) 1223-336-033; or E-mail: deposit@ccdc.cam.ac.uk.

Acknowledgements

S.G. thanks UGC for financial support in the form of a Minor Research Project [SPSW-044/09-10(ERO)]. The single crystal X-ray diffractometer used in this work has been funded by the Department of Science and Technology (DST-FIST), New Delhi, India, to the Department of Chemistry, J.U. The authors are thankful to UGC, New Delhi, for

funding UVP Bio Doc-IT GEL Imaging system in the form of a Major Research Project to KKM [39-706/2010(SR)].

References

[1] H.T. Chifotides, K.R. Dunbar. *Acc. Chem. Res.*, **38**, 146 (2005).
[2] H.Y. Sang, J.L. Byoung, H. Kim, J. Suh. *J. Am. Chem. Soc.*, **127**, 9593 (2005).
[3] G. Zuber, J.C. Quada Jr, S.M. Hecht. *J. Am. Chem. Soc.*, **120**, 9368 (1998).
[4] S.M. Hecht. *J. Nat. Prod.*, **63**, 158 (2000).
[5] V. Brabec, J. Malina, N. Margiotta, G. Natile, J. Kasparkova. *Chem. Eur. J.*, **18**, 15439 (2012).
[6] (a) R.N. Butenko, A.I. Tomaz, O. Nouni, E. Escribano, V. Moreno, S. Gama, V. Ribeiro, J.P. Telo, J.C. Pessoa, I. Caraco. *J. Inorg. Biochem.*, **103**, 622 (2009); (b) A. Silvestri, G. Barone, G. Ruisi, M.T. Lo Giudice, S. Tumminello. *J. Inorg. Biochem.*, **98**, 589 (2004).
[7] (a) C. Metcalfe, J.A. Thomas. *Chem. Soc. Rev.*, **32**, 215 (2003); (b) M. Navarro, E.J. Cisneros-Fajardo, A. Sierralta, M. Fernández-Mestre, P. Silva, D. Arrieche, E. Marchán. *J. Biol. Inorg. Chem.*, **8**, 401 (2003).
[8] L.J. Ignarro. *Hypertension*, **16**, 477 (1990).
[9] A. Calver, J. Collier, P. Vallance. *Exp. Physiol.*, **78**, 303 (1993).
[10] S.H. Snyder, D.S. Bredt. *Sci. Am.*, **266**, 68 (1992).
[11] A.P. Castano, P. Mroz, M.R. Hamblin. *Nat. Rev. Cancer*, **6**, 535 (2006).
[12] F. Doctorovich, F. Di Salvo. *Acc. Chem. Res.*, **40**, 985 (2007).
[13] J.E. Jee, S. Eigler, N. Jux, A. Zahl, R. van Eldik. *Inorg. Chem.*, **46**, 3336 (2007).
[14] T.E. Bitterwolf. *Coord. Chem. Rev.*, **250**, 1196 (2006).
[15] L.E. Goodrich, F. Paulat, V.K.K. Praneeth, N. Lehnert. *Inorg. Chem.*, **49**, 6293 (2010).
[16] T.C. Berto, V.K.K. Praneeth, L.E. Goodrich, N. Lehnert. *J. Am. Chem. Soc.*, **131**, 17116 (2009).
[17] J.A. McCleverty, M.D. Ward. *Compr. Coord. Chem. II*, **2**, 743 (2004).
[18] S.R. Choudhury, M. Selim, S. Chatterjee, S. Igarshi, Y. Yukawa, K.K. Mukherjea. *J. Coord. Chem.*, **65**, 3469 (2012).
[19] (a) B. Machura, J.O. Dziegielewski, T.J. Bartczak, J. Kusz. *J. Coord. Chem.*, **56**, 417 (2003); (b) B. Machura. *Coord. Chem. Rev.*, **249**, 2277 (2005); (c) B. Machura, R. Kruszynski, M. Jaworska. *Polyhedron*, **24**, 419 (2005).
[20] (a) N. Davies, M.T. Wilson, E. Slade, S.P. Fricker, B.A. Murrer, N.A. Powell, G.R. Henderson. *Chem. Commun.*, 47 (1997); (b) Y. Chen, R.E. Shepherd. *J. Inorg. Biochem.*, **68**, 183 (1997).
[21] M.H. Groothaert, J.A. Van Bokhoven, A.A. Battiston, B.M. Weckhuysen, R.A. Schoonheydt. *J. Am. Chem. Soc.*, **125**, 7629 (2003).
[22] S. Kuwata, S. Kura, T. Ikariya. *Polyhedron*, **26**, 4659 (2007).
[23] N.L. Fry, B.J. Heilman, P.K. Mascharak. *Inorg. Chem.*, **50**, 317 (2011).
[24] M.J. Rose, M.M. Olmstead, P.K. Mascharak. *J. Am. Chem. Soc.*, **129**, 5342 (2007).
[25] C.F. Edwards, W.P. Griffith, A.J.P. White, D.J. Williams. *J. Chem. Soc., Dalton Trans.*, 957 (1992).
[26] (a) Bruker. *APEX 2, SAINT, XPREP*, Bruker AXS Inc., Madison, WI (2007); (b) Bruker. *SADABS*, Bruker AXS Inc., Madison, WI (2001).
[27] SHELXS 97 and SHELXL 97, G.M. Sheldrick. *Acta Crystallogr., Sect. A: Found. Crystallogr.*, **64**, 112 (2008).
[28] C.K. Johnson. *ORTEP-III, Report ORNL – 5138*, Oak Ridge National Laboratory, Oak Ridge, TN (1976).
[29] J.J. McKinnon, A.S. Mitchell, M.A. Spackman. *Chem. Eur. J.*, **4**, 2136 (1998).
[30] M.A. Spackman, P.G. Byrom. *Chem. Phys. Lett.*, **267**, 215 (1997).
[31] J.J. McKinnon, M.A. Spackman, A.S. Mitchell. *Acta Crystallogr., Sect. B*, **60**, 627 (2004).
[32] S.K. Wolff, D.J. Grimwood, J.J. McKinnon, D. Jayatilaka, M.A. Spackman. *Crystal Explorer 2.1*, University of Western Australia, Perth (2007).
[33] J.J. Koenderink, A.J. van Doorn. *Image Vision Comput.*, **10**, 557 (1992).
[34] M.A. Spackman, J.J. McKinnon. *CrystEngComm*, **4**, 378 (2002).
[35] M.J. Frisch, G.W. Trucks, H.B. Schlegel, G.E. Scuseria, M.A. Robb, J.R. Cheeseman, J.A. Montgomery Jr, T. Vreven, K.N. Kudin, J.C. Burant, J.M. Millam, S.S. Iyengar, J. Tomasi, V. Barone, B. Mennucci, M. Cossi, G. Scalmani, N. Rega, G.A. Petersson, H. Nakatsuji, M. Hada, M. Ehara, K. Toyota, R. Fukuda, J. Hasegawa, M. Ishida, T. Nakajima, Y. Honda, O. Kitao, H. Nakai, M. Klene, X. Li, J.E. Knox, H.P. Hratchian, J.B. Cross, C. Adamo, J. Jaramillo, R. Gomperts, R.E. Stratmann, O. Yazyev, A.J. Austin, R. Cammi, C.J. Pomelli, W. Ochterski, P.Y. Ayala, K. Morokuma, G.A. Voth, P. Salvador, J.J. Dannenberg, V.G. Zakrzewski, S. Dapprich, A.D. Daniels, M.C. Strain, O.D. Farkas, K.A. Malick, D. Rabuck, K. Raghavachari, J.B. Foresman, J.V. Ortiz, Q. Cui, A.G. Baboul, S. Clifford, J. Cioslowski, B.B. Stefanov, G. Liu, A. Liashenko, P. Piskorz, I. Komaromi, R.L. Martin, D.J. Fox, T. Keith, M.A. Al-Laham, C.Y. Peng, A. Nanayakkara, M. Hallacombe, P.M.W. Gill, B. Johnson, W. Chen, M.W. Wong, C. Gonzalez, J.A. Pople. *GAUSSIAN 03 (Revision C.01)*, Gaussian Inc., Pittsburgh, PA (2004).

[36] (a) A.D. Becke. *J. Chem. Phys.*, **98**, 5648 (1993); (b) C. Lee, W. Yang, R.G. Parr. *Phys. Rev. B*, **37**, 785 (1988).
[37] G.A. Petersson, M.A. Al-Laham. *J. Chem. Phys.*, **94**, 6081 (1991).
[38] (a) P.J. Hay, W.R. Wadt. *J. Chem. Phys.*, **82**, 299 (1985); (b) P.J. Hay, W.R. Wadt. *J. Chem. Phys.*, **82**, 270 (1985); (c) W.R. Wadt, P.J. Hay. *J. Chem. Phys.*, **82**, 284 (1985).
[39] F. Eckert, A. Klamt. *J. AIChE*, **48**, 369 (2002).
[40] (a) S.I. Gorelsky. *AOMix, Program for Molecular Orbital Analysis*, University of Ottawa (2007), http://www.sg-chem.net/; (b) S.I. Gorelsky, A.B.P. Lever. *J. Organomet. Chem.*, **635**, 187 (2001).
[41] (a) S.R. Chowdhury, S. Dinda, S. Chakraborty, C. Simonnet, A.K. Mukherjee, K.I. Okamoto, R. Bhattacharyya. *Inorg. Chem. Commun.*, **8**, 61 (2005); (b) J. Smith, W. Purcell, G.J. Lamprecht, J.G. Leipoldt. *Polyhedron*, **14**, 1795 (1995).
[42] M.E. Reichmann, S.A. Rice, C.A. Thomas, P. Doty. *J. Am. Chem. Soc.*, **76**, 3047 (1954).
[43] J. Marmur. *J. Mol. Biol.*, **3**, 208 (1961).
[44] A. Wolfe, G.H. Shimer, T. Meehan. *Biochemistry*, **26**, 6392 (1987).
[45] M. Selim, K.K. Mukherjea. *J. Biomol. Struct. Dyn.*, **26**, 561 (2009).
[46] J.B. Chaires, N. Dattagupta, D.M. Crothers. *Biochemistry*, **21**, 3933 (1982).
[47] D. Mustard, D.W. Ritchie. *Protein: Struct., Funct., Bioinf.*, **60**, 269 (2005).
[48] (a) R.D. Feltham, J.H. Enemark. *Top. Stereochem.*, **12**, 155 (1981); (b) W.P. Griffith, P.M. Kierman, J.-M. Brégeault. *J. Chem. Soc., Dalton Trans.*, 1411 (1987); (c) S. Sarkar, P. Subramanian. *Inorg. Chim. Acta*, **35**, L357 (1979).
[49] (a) R. Bhattacharyya, P.S. Roy, A.K. Dasmahapatra. *J. Chem. Soc., Dalton Trans.*, 793 (1988); (b) D. Fenske, N. Mronga, K. Dehnicke. *Z. Anorg. Allg. Chem.*, **498**, 131 (1983); (c) J.A. Casey, R.K. Murmann. *J. Am. Chem. Soc.*, **92**, 78 (1970); (d) P.T. Manoharan, H.B. Gray. *Inorg. Chem.*, **5**, 823 (1966).
[50] (a) B.A. Goodman, J.B. Raynor, M.C.R. Symons. *J. Chem. Soc. A*, 994 (1966); (b) P.T. Manoharan, H.B. Gray. *Chem. Commun.*, 324 (1965).
[51] P.O. Lumme, U. Turpeinen. *Acta Crystallogr., Sect. C*, **47**, 501 (1991).
[52] J.O. Dziegielewski, B. Machura, T.J. Bartczak, W. Czurak, J. Kusz, J. Warczewski. *J. Coord. Chem.*, **48**, 125 (1999).
[53] (a) J.O. Dziegielewski, B. Machura, J. Marke. *Polyhedron*, **15**, 3713 (1996); (b) A. Muller, M. Ishaque Khan, E. Krickemeyer, H. Bogge, *Inorg. Chem.*, **30**, 2040 (1991).
[54] (a) J.H. Enemark, M.S. Quinby, L.L. Reed, M.J. Steuck, K.K. Walthers. *Inorg. Chem.*, **9**, 2397 (1970); (b) J.H. Enemark, R.D. Feltham. *Coord. Chem. Rev.*, **13**, 339 (1974); (c) B. Machura, M. Jaworska, R. Kruszynski. *Polyhedron*, **23**, 1819 (2004).
[55] M.A. Spackman, D. Jayatilaka. *CrystEngComm*, **11**, 19 (2009).
[56] J.K. Barton, A. Danishefsky, J. Goldberg. *J. Am. Chem. Soc.*, **106**, 2172 (1984).
[57] T.M. Kelly, A.B. Tossi, D.J. McConnell, T.C. Strekas. *Nucleic Acids Res.*, **13**, 6017 (1985).
[58] F. Schaeffer, S. Rimsky, A. Spassky. *J. Mol. Biol.*, **260**, 523 (1996).
[59] T.K. Si, S.S. Paul, M.G.B. Drew, K.K. Mukherjea. *Dalton Trans.*, **41**, 5805 (2012).
[60] S. Patra, S. Chatterjee, T.K. Si, K.K. Mukherjea. *Dalton Trans.*, **42**, 13425 (2013).
[61] (a) Y.M. Song, Q. Wu, P.J. Yang, N.N. Luan, L.F. Wang, Y.M. Liu. *J. Inorg. Biochem.*, **100**, 1685 (2006); (b) C. Tan, J. Liu, L. Chen, S. Shi, L. Ji. *J. Inorg. Biochem.*, **102**, 1644 (2008).
[62] (a) S.S. Paul, M. Selim, A. Saha, K.K. Mukherjea. *Dalton Trans.*, **43**, 2835 (2014) (doi: 10.1039/C3DT52434E); (b) J.R. Lakowicz, G. Weber. *Biochemistry*, **12**, 4161 (1973).
[63] J. Liu, T. Zhang, T. Lu, L. Qu, H. Zhou, Q. Zhang, L. Ji. *J. Inorg. Biochem.*, **91**, 269 (2002).
[64] S. Satyanarayana, J.C. Dabrowiak, J.B. Chaires. *Biochemistry*, **31**, 9319 (1992).
[65] P. Wittung, P. Nielsen, B. Norden. *J. Am. Chem. Soc.*, **118**, 7049 (1996).
[66] M. Selim, S.R. Choudhary, K.K. Mukherjea. *Int. J. Biol. Macromol.*, **41**, 579 (2007).
[67] (a) T.A. Dix, K.M. Hess, M.A. Medina, R.W. Sullivan, S.L. Tilly, T.L.L. Webb. *Biochemistry*, **35**, 4578 (1996); (b) T.H. Zastawny. *Free Radical Biol. Med.*, **18**, 1013 (1995); (c) P. Tachon. *Free Radical Res. Commun.*, **7**, 1 (1989); (d) P. Tachon. *Free Radical Res. Commun.*, **9**, 39 (1990); (e) J.H. Kang. *Bull. Korean Chem. Soc.*, **31**, 2873 (2010).
[68] H. Ihtshamul, J. Ladbury. *J. Mol. Recognit.*, **13**, 188 (2000).
[69] M. Baginski, F. Fogolari, J.M. Briggs. *J. Mol. Recognit.*, **274**, 253 (1997).
[70] E.M. Proudfoot, J.P. Mackay, P. Karuso. *Biochemistry*, **40**, 4867 (2001).
[71] R. Filosa, A. Peduto, S. Di Micco, P. de Caprariis, M. Festa, A. Petrella, G. Capranico, G. Bifulco. *Bioorg. Med. Chem.*, **17**, 13 (2009).